The Effect of Internal Wave-Related Features on Synthetic Aperture Sonar

Roy Edgar Hansen, *Member, IEEE*, Anthony P. Lyons, *Member, IEEE*,
Torstein Olsmo Sæbø, *Senior Member, IEEE*, Hayden John Callow, *Member, IEEE*,
Daniel A. Cook, *Senior Member, IEEE*

***Abstract*—In October 2012, the Centre for Maritime Research and Experimentation (CMRE) conducted trials from the NATO research vessel Alliance, off of Elba island, Italy. During this trial, data was collected by the Norwegian Defence Research Establishment (FFI) using a HUGIN autonomous underwater vehicle (AUV) with interferometric synthetic aperture sonar (SAS) in repeated passes. Large linear structures (tens of meters by several meters) observed in both the SAS images and SAS bathymetry during the initial pass were absent in data taken on a repeated pass the following day. We suggest that these phenomena were not true seafloor features, but were caused by features in the water column, known as boluses, which can form after breaking internal wave events. The changes observed in acoustic intensity and phase appear to be caused by the interaction of the acoustic field with the lower average sound speed structure of the bolus, constructing features in both SAS imagery and SAS bathymetry that looked like seabed topography. In this paper we present examples and give an interpretation of the results based on an acoustic ray model. We discuss different techniques for recognizing these phenomena: Repeat pass imaging and interferometry, multi-look and multi-aperture processing, and moving target analysis.**

***Index Terms*—Synthetic aperture sonar, internal waves, refraction effects**

Fig. 1. The HUGIN autonomous underwater vehicle with the HISAS wideband interferometric synthetic aperture sonar during launch from NATO research vessel Alliance in October 2012.

I. Introduction

SYNTHETIC aperture sonar (SAS) is a major tool for seabed imaging and mapping, providing very fine resolution and high image quality. Although SAS technology today is well known and has a long history, it is only within the last decade that it has matured substantially and become more readily available [1], [2]. As in synthetic aperture radar (SAR) [3], [4], SAS is a technique that produces images that are well suited for estimating coherent or noncoherent changes over repeated passes, a technique known as *change detection* [5].

All types of sonar are affected by the ocean environment, and the vertical sound speed profile is particularly influential [6]. In SAS, the two most dominant effects caused by incorrect knowledge of the sound speed are defocusing, especially for widebeam systems [7], [8], and bias in the seabed depth estimation using interferometry. The latter is also a common issue for multibeam echosounders [6]. Strong variability in the ocean sound speed structure induced by internal waves or turbulence also exists, and can limit the temporal and spatial coherence of acoustic signals in sonar [9]. Experiments have shown that this problem in many cases is not large enough to be restrictive in SAS [10], [11]. At present, most SAS processing algorithms also use data driven navigation (known as micronavigation) [12] to achieve the required position accuracy for successful SAS imaging. Micronavigation will inherently reduce the effect of the variability in the water column in SAS [13].

In October 2012, the Centre for Maritime Research and Experimentation (CMRE) conducted the ARISE'12 trials from the NATO research vessel Alliance, off of Elba island, Italy. During this trial, change detection data was collected by the Norwegian Defence Research Establishment (FFI) using a HUGIN autonomous underwater vehicle (AUV) with interferometric SAS (see Fig. 1). Large linear structures (tens of meters by several meters) in the SAS images and in the SAS bathymetry apparently disappeared or changed in repeated passes with 28 hour time separation. These changes were present near a depth where a strong density and sound speed step intersected the sloping seafloor. The weather was calm and the sea state was low during the trial period. Similar features were observed multiple times over several days in the same

Revised manuscript received June 6, 2014

R. E. Hansen and T. O. Sæbø are with the Norwegian Defence Research Establishment (FFI), P.O. Box 25, N-2027 Kjeller, Norway.

A. P. Lyons is with the Applied Research Laboratory, Penn State University, University Park, PA 16804, USA.

H. J. Callow is with Kongsberg Maritime, NO-3191 Horten, Norway.

D. A. Cook is with Georgia Tech Research Institute, Atlanta, GA 30332, USA

Corresponding author: Roy-Edgar.Hansen@ffi.no.

DOI til publisert versjon / DOI to published version: 10.1109/JOE.2014.2340351

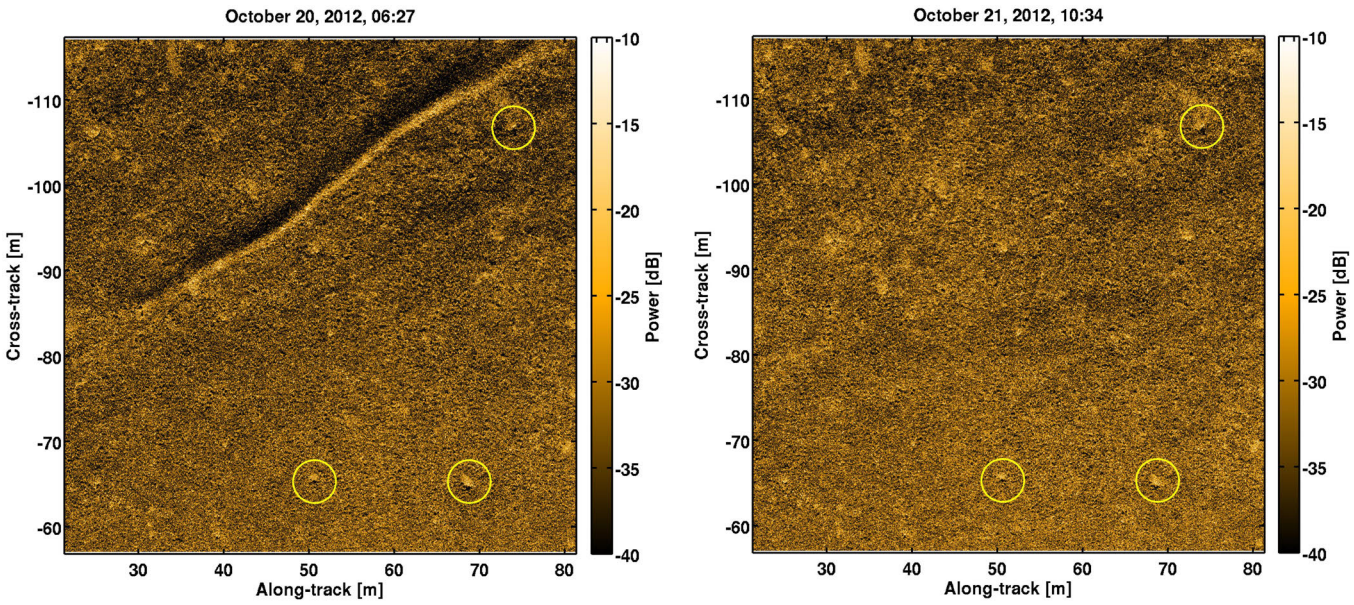

Fig. 2. SAS images of the same scene taken on 20 and 21 October 2012, 28 hours apart. The left image is the earliest. The yellow circles highlight small rocks in the scene indicating that the images are accurately co-registrated.

area.

We suggest that these anomalies in the SAS images and the SAS bathymetry estimates were not caused by changes in the seafloor, but by water column features known as boluses which result from breaking internal waves [14]–[17]. Internal wave boluses are formed after an internal wave breaking event captures colder water within a small area surrounded by warmer water. These internal wave boluses then move slowly up-slope along the seabed. The changes observed in acoustic intensity and phase can be described by refraction as propagating acoustic waves interact with the variation in sound speed caused by the bolus. Our interpretation of this phenomenon is based on a ray model that describes the variation in backscattered intensity from the seabed as a focusing of sound by the bolus, and describes the error in the SAS bathymetry by the refractive effect caused by the bolus. A similar effect has been documented in airborne SAR [18]–[20].

In Section II we show SAS images and bathymetries of the phenomena. In Section III we apply a simple ray acoustic model to describe the refractive effects from such anomalies in the water column. Section IV lists potential techniques to establish if a feature in a SAS image is a true feature on the seabed or an artificial feature caused by refractive effects. Finally, we summarize the findings in Section V.

II. Illustration of the Phenomena

The HISAS 1030 is a programmable wideband interferometric SAS suitable for high resolution imaging and mapping of the seabed [8], [21]. The sensor is operated from HUGIN AUVs at a typical vehicle altitude above the seabed of $10 - 20$ m. All data examples in this paper are collected with this sensor. Table I summarizes the key system specifications during the experiment. The images are created using the backprojection algorithm in ground coordinates, after micronavigation is applied [8].

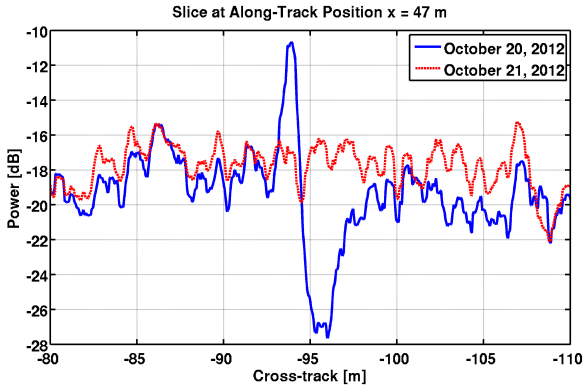

Fig. 3. Slice through the images shown in Fig. 2 at $x = 47$ m.

The left panel of Fig. 2 shows a SAS image covering 60×60 m of the seabed at approximately 46 m water depth. The theoretical along-track and across-track resolution in the image is 3.7×3.3 cm. The right panel shows a SAS image made of the same scene 28 hours later. The yellow circles in the two images indicate small rocks that are present in both images. The images are co-registered to sub-pixel accuracy [22], [23].

TABLE I
System specifications during the data acquisition.

Center frequency	100 kHz
Wavelength	1.5 cm
Bandwidth	30 kHz
Interferometric baseline	30 cm
Along-track resolution	< 4 cm
Cross-track resolution	< 4 cm
Maximum range @ 2 m/s	200 m

Dette er en postprint-versjon / This is a postprint version.
DOI til publisert versjon / DOI to published version: 10.1109/JOE.2014.2340351

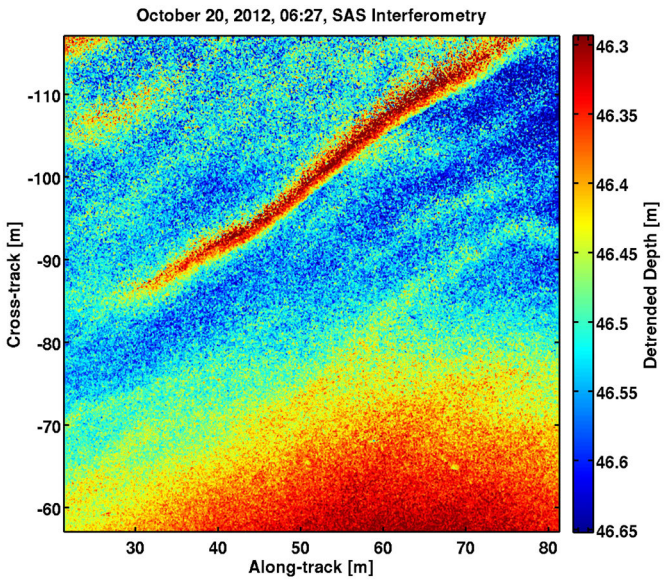

Fig. 4. Seabed depth estimate from SAS interferometry based on the image shown in the left panel in Fig. 2. The average slope has been removed.

The large diagonal feature in the top portion of the left panel is entirely consistent with intensity variations caused by slope changes from a ridge of sand. The apparent ridge is absent in the image collected 28 hours later. The sea state during the period was low and so sediment transport could not remove such a large feature.

Figure 3 shows the intensity profile slice from both images in Fig. 2 at along-track position $x = 47\,\mathrm{m}$. The profiles are calculated by averaging over 2 m along-track and applying a 26 cm boxcar averaging across-track. The intensity variation caused by the phenomenon is 6 dB stronger in the highlight region and 10 dB weaker in the shadow region. These are strong variations and would be easily seen as an anomaly in change detection.

The sensor used in the experiment contains two vertically offset receiver arrays allowing for single pass SAS interferometry. Figure 4 shows the estimate of the seabed depth from the interferometric processing in the presence of the suspected internal wave bolus shown in the left panel of Fig. 2. The average slope of the seabed is removed (the data are detrended). We have performed the interferometric processing with the weighted multiband split-spectrum algorithm and an $18 \times 18\,\mathrm{cm}$ interferogram estimation window [24]. The map shows a ridge-shape with a seabed depth profile that would be expected from the variation in the backscattered intensity shown in the SAS image. The interferometric coherence [25, chapter 4.3] is high, indicating that the interferometric image pairs are accurately co-registered and that there are valid backscattered signals in the full scene including the apparent shadow region. In the repeated pass seabed depth estimate there is no visible sign of the feature (similar to the repeated pass intensity image shown in Fig. 2).

Figure 5 shows profiles of estimated seabed depth from SAS bathymetry taken on both days at an along-track position $x = 47\,\mathrm{m}$ (the same position as the profiles displayed in Fig. 3). In the profile with the suspected bolus present, the estimated height of the apparent ridge is seen to be approximately $20 - 30\,\mathrm{cm}$. We also see that the apparent depth slope after the internal wave feature is different between the two days. This can be explained by small changes in the thermocline between the passes, and ignoring the refraction effect in the interferometric processing. Refraction effects are discussed in detail in the next section.

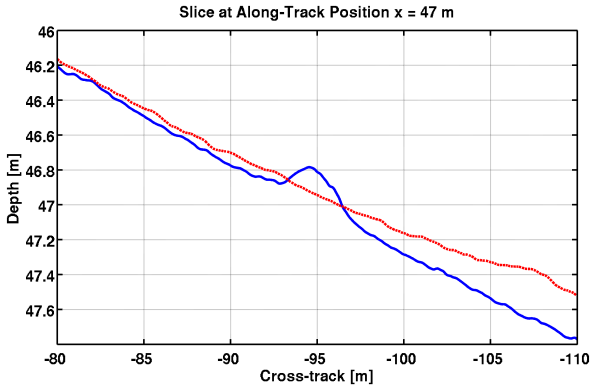

Fig. 5. Slice through the bathymetry shown in Fig. 4 compared with the repeated pass at $x = 47\,\mathrm{m}$.

III. Acoustic Refractive Model

Figure 6 shows the average temperature profile, density profile, and sound speed profile based on CTD measurements taken October 20, 2012, in the trial area. There is a strong step change in both the density and the sound speed from around 40 m depth to 60 m depth, caused by a seasonal thermocline which is common in the Mediterranean in the late summer and early fall. This large gradient create conditions suitable for propagating internal waves and consequently refractive effects on acoustic wave propagation. For the data example in the previous section, the sloping seabed intersects with the density step similarly as in [17] indicating the possibility of existence of internal wave boluses.

In order to understand how a water column effect can cause features similar to our observations, we develop a simple ray model. We follow [15] and assume a simplified parabola shaped wave feature of cold dense water with sound speed c_1

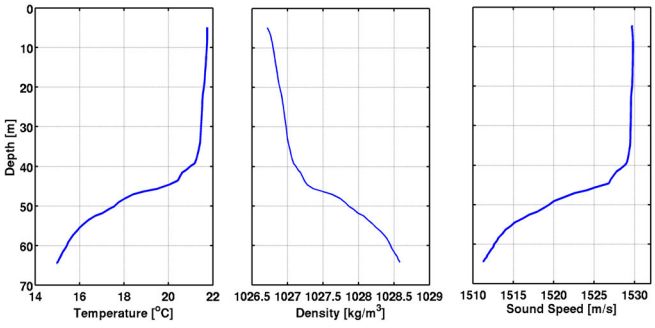

Fig. 6. Temperature, density and sound speed profile taken during the experiment.

Dette er en postprint-versjon / This is a postprint version.
DOI til publisert versjon / DOI to published version: 10.1109/JOE.2014.2340351

and density ρ_1 lying on the seabed surrounded by warmer lighter water with sound speed c_0 and density ρ_0. This is illustrated in Fig. 7. Following [26, chapter 3.1], the reflection coefficient for normal incidence is

$$V = \frac{m-n}{m+n}, \text{ where } m = \frac{\rho_1}{\rho_0}, \text{and } n = \frac{c_1}{c_0} \tag{1}$$

For the case shown in Fig. 6, we have $c_0 = 1530\,\text{m/s}$, $c_1 = 1510\,\text{m/s}$, $\rho_0 = 1028.5\,\text{kg/m}^3$, $\rho_1 = 1027\,\text{kg/m}^3$. This gives a reflection coefficient of $V \approx 0.007$, indicating that backscattering from the internal wave itself is very difficult to detect if not impossible for a sidelooking sonar geometry. Echoes from the seabed will also be present at the same slant range as the internal wave, and they will most likely mask the potential echo from the internal wave itself. Note that this is different from the observations documented in [17], where a narrowbeam downwards looking sonar was used.

It is straightforward to apply Snell's law of refraction for each ray at each of the interfaces between cold and warm water. For convex surfaces encapsulating lower sound speeds, incoming horizontal acoustic rays from a source will be refracted towards the seabed. The effect in the image will be a function of the sound speed difference, the exact size and shape of the feature, and geometry. We perform a simple calculation to illustrate the effect. Assume a parabolic shape of height H and width L filled solely with water of sound speed c_1. The vertical shape boundary is described by

$$z = -\frac{H}{(L/2)^2}y^2 + H, \quad \frac{dz}{dy} = -\frac{2H}{(L/2)^2}y \tag{2}$$

where z is the vertical position and y is the horizontal position (across-track ground range). The derivative and thereby the normal vector is known at each position of the parabola. This can be used in calculating all the angles involved. The individual rays can be traced through the parabola by applying Snell's law.

In [15] the typical shape of the bolus was found to have $H/L \approx 0.3$. Our initial studies [27] suggested that the bolus height (or amplitude) could be around $1.5 - 3\,\text{m}$. In this simulation, we have chosen $H = 1.25\,\text{m}$, $L = H/0.3$ to fit the observed shadow length in the data. Figure 8 shows the results from our simple ray model. We have chosen incoming rays with an incidence angle of $\theta \approx 16/100 \approx 9°$. This is approximately correct for the data example in Fig. 2 with the corresponding geometry sketched in Fig. 7. Note that

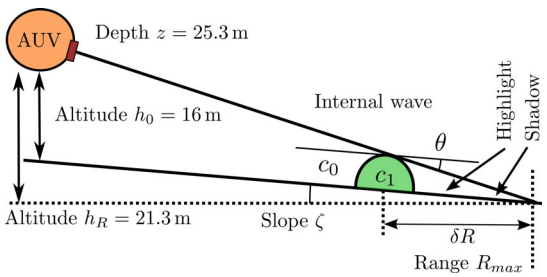

Fig. 7. Vertical geometry of the imaging through an internal wave bolus on a sloping seabed.

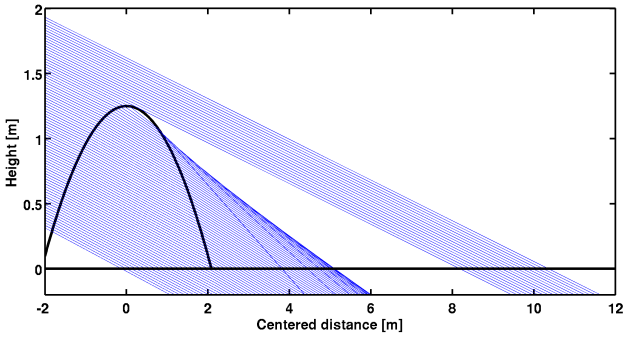

Fig. 8. Interaction of acoustic rays with a parabola containing lower sound speed. Note that the aspect ratio in the plot is not 1:1, causing the rays to appear steeper than what they are.

the seabed itself is sloping with $\zeta = (h_R - h_0)/R_{max} \approx 5.3/100 \approx 3°$. The rays that intersects close to the top of the parabola are the rays that refract downwards the most. This refraction caused by the bolus gives the *lens effect* as described in [20].

From the ray model, it is possible to describe four different effects that may be observed in the SAS images and bathymetry:

1) The ray density on the seabed varies due to the refraction effect. In the upper panel of Fig. 9, we show the ray density for the case shown in Fig. 8. The ray density is normalized with respect to the ray density of a homogeneous water column. We see that the ray density increases rapidly and by a factor of 3 until the shadow region appears. This corresponds to approximately 9 dB increase in relative power, but on a very confined small range interval.
2) The increase of grazing angle due to ray steepening will cause a change in scattering strength. There exists various models for roughness scattering from the seabed [28, chapter 13]. Since these effects are observed close to grazing incidence, a small roughness perturbation approximation model may be used. The center panel of Fig. 9 shows the grazing angle as function of distance from parabola. Since the refractive effect from the parabola causes rays to cross, there will be multiple grazing angles in a certain range interval. There are, however, very few rays with steep angles due to the small amount of rays intersecting with the top part of the parabola. Around the maximum ray density, the grazing angle changes from $9°$ to around $13°$. This corresponds approximately to a difference in backscattering strength of 5 dB for sand seabed types and 3 dB for silt/clay seabed types, when applying the system and the geometry to the APL-UW94 scattering model [29].
3) In the interferometry processing, the seabed topography is estimated from the acoustic ray direction of arrival [25], [30]. The non-linearity of the rays will cause an error in the SAS interferometric bathymetry. The error may occur even when the interferometric coherence is very high. Refraction induced errors are a common problem for other bathymetric sensors such as multibeam

Dette er en postprint-versjon / This is a postprint version.
DOI til publisert versjon / DOI to published version: 10.1109/JOE.2014.2340351

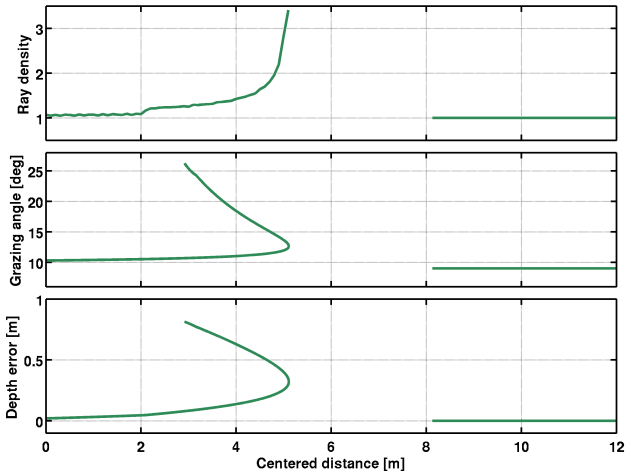

Fig. 9. Ray density (upper), grazing angle (center), and refraction induced interferometric depth error for the acoustic rays interacting with the parabola in Fig. 8.

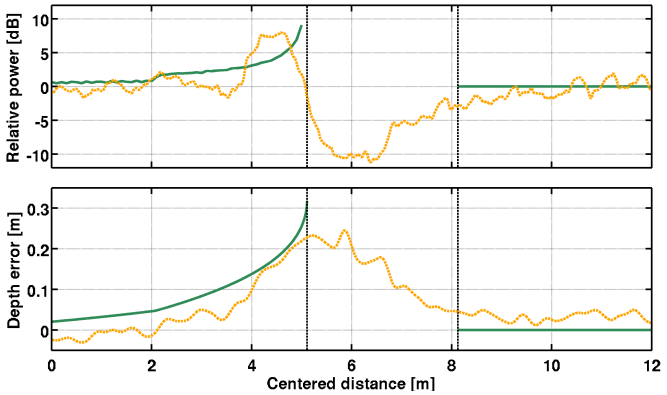

Fig. 10. Upper: Modeled signal power (green) compared with measured signal difference. Lower: Modeled depth error caused by refraction compared with detrended measured depth.

echosounders [6]. The lower panel of Fig. 9 shows the depth error caused by ray non-linearity for the model case in Fig. 8. As with the grazing angle, there are two conflicting depths for certain distances from the parabola. The largest depth errors (around 0.8 m value) are caused by very few rays, and may not be observable. The depth error around the maximum ray density which corresponds to the peak in signal intensity, is around 0.3 m.

4) The lowered sound speed c_1 within the parabola will cause a displacement error in the SAS image. The rays that propagate through the parabola will be slowed down slightly such that the texture and speckle in the SAS image behind the parabola will be displaced. This effect will be largest for the rays that intersects the parabola close to the seabed and thereby refracts the least. To get a rough estimate of the effect, we assume a ray that intersects the parabola at the half-height of the parabola $H/2$. The approximate horizontal distance through the parabola becomes $\delta L \approx 3.5\,\mathrm{m}$, giving a displacement error

$$\delta r \approx \delta L(1 - c_1/c_0) \approx 4.5\,\mathrm{cm}. \quad (3)$$

Note that the ray refraction will also cause displacement in the image, but not as much as that due to lowered sound speed.

These four effects may be used for detecting internal wave boluses in SAS data, and they may also be used to invert for internal wave parameters. There are three noticable effects that will affect the measurements: In our simulated scenario, we use a perfect parabola-shaped bolus. In reality the shape may be different, and mixing of the water outside and inside the parabola may occur. The second effect lies in the horizontal plane. SAS imaging uses the angular spread over multiple pings to obtain finer along-track resolution. Hence, a bolus will be sampled at different horizontal look angles in one SAS image. Acoustic waves that propagate through the internal wave boluses may also be refracted horizontally. Finally, the geometry will affect the measurements. A non-planar seabed topography will cause the internal wave bolus to change direction, shape and speed, and the SAS data collection will be from an ensemble of geometries as described by the model.

Due to the sum of all these effects, measurements are expected to contain less extreme boundaries and peak values: in the shadow region, there will still be some signal; the peak depth error will be less than the modeled; the peak signal strength will be less than the modeled; and the far end transition between shadow and normal backscatter behind the affected area will be softened (around centered distance of 9 m in Fig. 8).

The upper panel of Fig. 10 shows the measured intensity difference between the two passes shown in Fig. 3 compared with the modeled ray density. The model results are positioned such that the shadow part fits the measurements. The lower panel shows the detrended SAS bathymetry from Fig. 5 compared with the modeled refraction induced depth error. The vertical bars indicate the boundaries of the modeled region where ray theory would give no intensity. We have removed the rays that are steeper than the angle at the maximum ray density (the turning point in Fig. 9). There is non-zero energy in the shadow region as well as valid bathymetry estimates, likely due to the effects discussed above.

IV. Recognition of Internal Wave Phenomena

As we have documented in Section II, the refractive effect of the internal waves can cause artificial structures. In sidescan images, regular SAS images, and in SAS bathymetry, these structures appear as one would expect a true topography feature to appear and are thus very difficult to differentiate from true topography. It is important to establish whether it is possible to detect or distinguish a water column induced feature from one that is actually a true seabed feature. In this section we list candidate techniques for recognition of these features, and show example results.

The basic assumption we start with follows the study of the refractive effect in Section III. For these internal waves to

Dette er en postprint-versjon / This is a postprint version.
DOI til publisert versjon / DOI to published version: 10.1109/JOE.2014.2340351

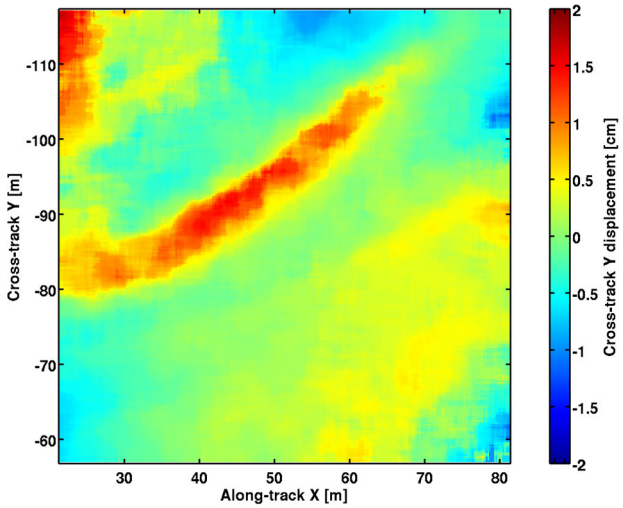

Fig. 11. Repeat pass interferometry between the two images in Fig. 2. Estimated y-shift (cross-track) in centimeters. The color represents the interval $[-2, 2]$ cm for the displacement.

create artificial features in the images, a few general conditions must be fulfilled:

- The ocean environmental conditions should be correct for the existence of internal waves and boluses that produce gradients of the correct shape (convex) in both density and sound speed.
- The sonar depth and orientation towards the seabed must allow for such features to be visible.
- The oceanographic features should move slowly.

When these three conditions are fulfilled, certain apparent structures (ridges and similar) in the sonar images can be created by refractive effects from these internal wave-related features. All three of these conditions were met during the Elba Island experiment in October, 2012.

A. Repeat Pass Imaging and Interferometry

The refractive effect of the assumed internal wave boluses are clearly visible and detectable when running controlled repeated passes where the vehicle track is very similar in each pass. A noncoherent image based change detection technique [31] is sufficient for detection of the waves. Repeat pass imaging and mapping in a controlled fashion, where images of the same scene from the same look angle are made repeatedly with a suitable temporal baseline, would be ideal for detection, mapping, and characterization of the internal wave-related phenomena.

Repeat pass interferometry in SAR [4], [25] uses images in repeated passes to estimate the topography as well as changes both in terrain and in the images. For stationary scenes and controlled data acquisition coherent change detection [22] may be applied, where changes not visible in the magnitude images can be detected. Note that the ocean environment may be a time-varying medium that changes the seabed such that there is a natural temporal decorrelation time for the seabed itself [32]. For sufficiently high repeat pass coherence, the apparent displacement of the backscattered signal (the speckle) for the signal that propagates through the water column feature can be estimated.

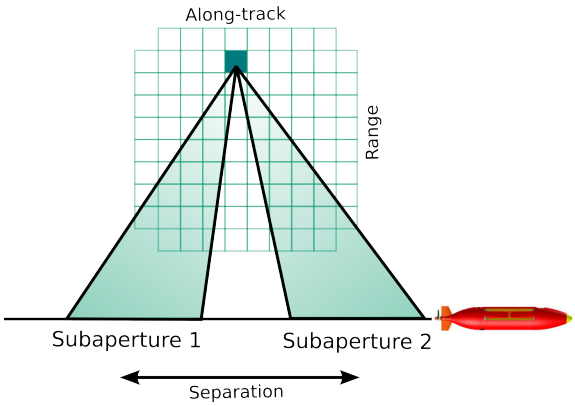

Fig. 12. Principle of multi-aperture SAS imaging.

Following the technique described in [33], we have performed repeat pass interferometry processing on the two images shown in Fig. 2. Figure 11 shows the estimated shift along the ground range axis (the y-axis). The results are median filtered to emphasize the effect of large scale motion. The average repeat pass coherence is 0.485 for these data. The results indicate a slowdown of the rays travelling through the assumed internal wave bolus that displaces the backscattered signal behind the feature around $1.5\,\text{cm}$. This is, as expected, lower than the modeled shift in Section III.

B. Multi-Aperture with Temporal Separation

Often the data collection only contains a single image (or a single pass), so the techniques discussed in the previous section cannot be used. If only a single pass is available, an intuitive technique is to divide the total length of the synthetic aperture into subapertures with a certain temporal separation as illustrated in Fig. 12. This is a well-known technique in the SAS field [34], [35], where the reason for doing this is to obtain images of different aspect angle on a potential target. In this particular case, we use a common imaging grid where non-overlapping pings are used in each subaperture image [36].

There is a fundamental disadvantage of using this technique. A shorter synthetic aperture will lead to poorer along-track resolution. In the case of detection of moving internal wave features, the main parameter is the temporal baseline (or separation). The wave is expected to move on the order of $5 - 10\,\text{cm/s}$ [27]. In order to use this technique, one must therefore choose a suitable temporal baseline which gives reasonable probability to detect the wave movement.

Figure 13 shows two sub-aperture images of one of the suspeced internal wave boluses at far range. The yellow lines are at fixed positions serving as guidelines for detection of wave movement. In this particular case, the temporal separation between the images is $21\,\text{s}$, and the integration time per image is $20.5\,\text{s}$. We see that the wave feature has moved between the temporal looks, although not clearly. A small investigation of this movement indicates that the wave phenomenon has

Dette er en postprint-versjon / This is a postprint version.
DOI til publisert versjon / DOI to published version: 10.1109/JOE.2014.2340351

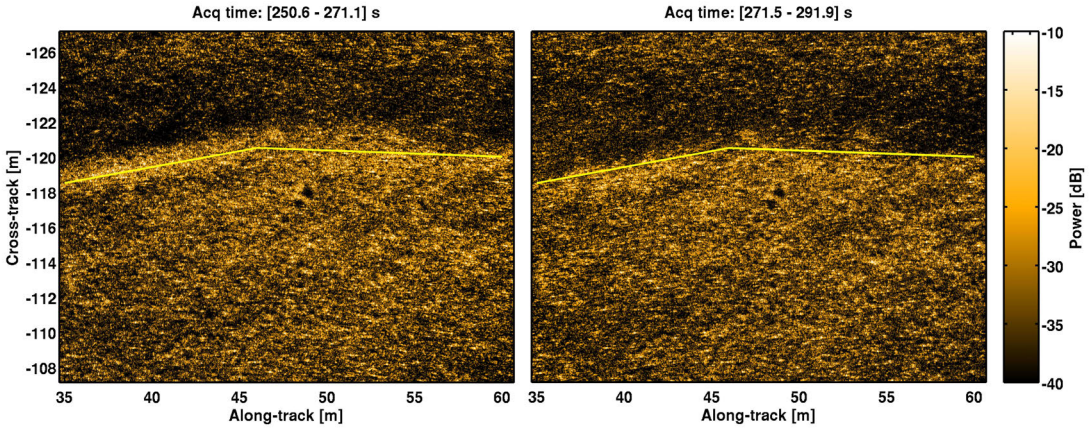

Fig. 13. Multi-aperture SAS images of the internal wave phenomenon. The yellow line is in fixed position in both images.

moved approximately $65\,\mathrm{cm}$ (maximally), which equals an estimated wave speed of $3\,\mathrm{cm/s}$. There is, however, a potential source for error in this analysis. Images from non-overlapping temporal sub-apertures may have differences in the horizontal wavenumber coverage (see section IV-C). This might lead to misinterpretation between wave movement and the refractive effects caused by the features as observed with different wavenumber coverages.

C. Multi-Look from Wavenumber Filtering

A similar, although not identical, technique to the one proposed in Section IV-B is to divide the wavenumber spectrum into sections and form images from each of them [3, chapter 3.8]. This is known in the SAR and SAS communites as multilook processing, as the properites of randomly distributed scatterers ensure that each look contains essentially the same scene [23, chapter 3.3]. Multilooking is usually used as a means of reducing speckle. However, potential wavenumber dependence in the scene content (i.e. where the holographic property is not fulfilled [23, chapter 3.3]), can be exploited to infer additional information. The most common example of this in spotlight-mode SAR is to divide the collection into subapertures to better observe moving target signatures and other changes happening on short time scales [37].

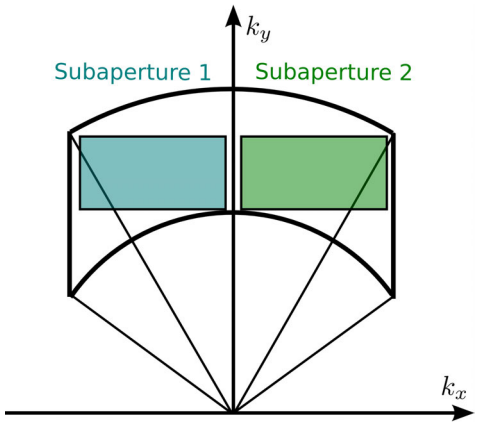

Fig. 14. Principle of multi-look from wavenumber filtering.

Interestingly, temporal and wavenumber subapertures are roughly equivalent for spotlight mode. However, there is a clear distinction between the domains for stripmap synthetic aperture data collections [3, chapter 1.3]. One may choose temporal subapertures as in Section IV-B or wavenumber subapertures. The latter can be thought of as angular filters. Consider the division shown in Fig. 14. The images resulting from these two subapertures would contain the same scene content and have the same interval of collection time. However, one image would correspond to a forward-looking beam, and the second to an aft-looking beam. Such imagery is useful for detecting internal waves only if there is a detectable change in refraction when the wave is viewed from different angles.

We might also multilook in the range wavenumber dimension. The resulting images will again possess identical content for areas obeying the holographic property. This time however, effects that vary with frequency, rather than angle, will induce differences between the images. The implication for detecting internal waves is the subject of ongoing research. The ray model of propagation indicates that the acoustic path is effectively independent of frequency. However, the coherent interference of the rays is a function of frequency, and thus may offer a means of detecting internal waves.

It is conceivable that internal waves can cause differences between images created from spectral subapertures. The question of determining the conditions under which these differences can be detected and measured remains to be answered. One difficulty is the fact that the subaperture images cannot be coherently compared because each contains an independent realization of the speckle. Detection must therefore rely on less sensitive approaches based on changes in image intensity. The variation between subapertures may be very slight, rendering the internal waves virtually undetectable using this method.

D. Backscatter and Topography Comparison

The refractive effect of an internal wave bolus will cause changes in the backscattered signal and the estimated seabed topography from interferometry (see Section III). A potential

Dette er en postprint-versjon / This is a postprint version.
DOI til publisert versjon / DOI to published version: 10.1109/JOE.2014.2340351

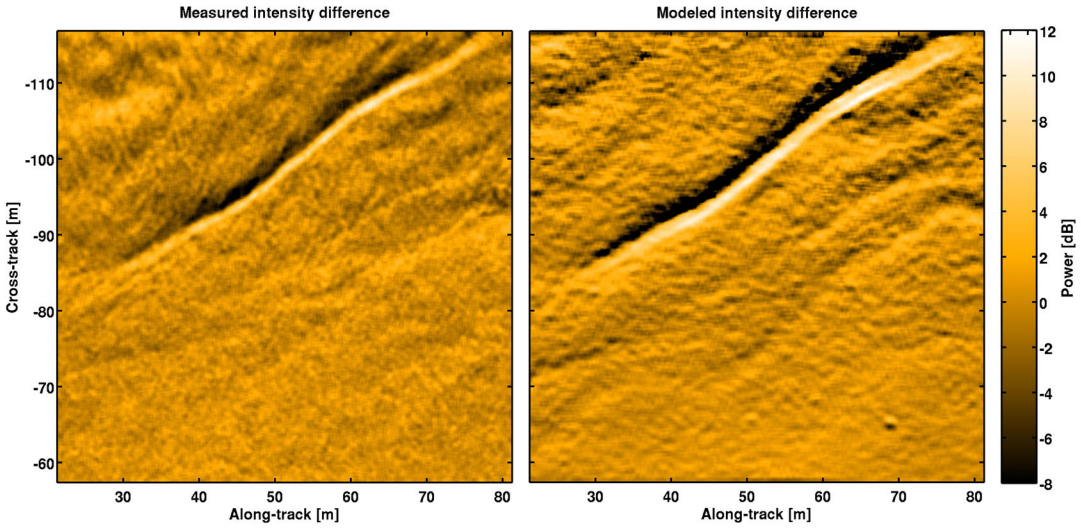

Fig. 15. Measured intensity difference (left) compared with modeled intensity difference from topography and slope change (right).

technique is then to compare the measured backscattered signal with a signal that would be backscattered from the estimated seabed topography. A misfit between the two can potentially be used to classify a feature as water column induced.

We have examined this technique on the suspected internal wave bolus shown in Fig. 2. We have calculated the expected backscattered diffference from the estimated topography difference based on the interferometry estimates from the two passes. Perturbation theory [28] was used to model the backscattered intensity. We can compare the estimated difference with the measured backscatter difference between the two passes. In this example, we have despeckled the results to emphasize the water column effect. The modeled and measured backscatter difference images are shown in Fig. 15. There are differences in the two images. Particularly, the modeled backscatter difference shows the wave patterns more clearly. This is due to lower variance in the estimated bathymetry compared to the estimated backscatter and thereby more easily detectable small changes (compare Fig. 3 with Fig. 5). Another noticable difference is that the modeled highlight and shadow contrast is stronger than the measured. This indicates leakage of acoustic signal into the shadow region (as also shown in Fig. 10). Whether these difference are substantial enough for reliable detection of water column induced features, remains unclear. Note that there is a fundamental limitation to this technique: The seabed type has to be known within certain bounds, modeled with a sufficiently accurate model, and not change over the scene that is investigated. This is the same limitation one encounters in *shape-from-shading* type processing [38].

E. Along-Track Interferometry

Repeat pass interferometry (see Section IV-A) is based on constructing interferograms representing phase and magnitude differences between co-registered images from repeated passes with a temporal separation (or baseline) that is suitable for studying the changes in the scene. One possibility is to use redundant transmitter/receiver elements to form two or more individual and co-registererd synthetic aperture images from a single pass (multi-channel synthetic apertures). This gives a very short temporal baseline (down to one pulse repetition) between the images. There are several approaches for detecting changes and moving objects in single-pass multi-channel imags: *Along-track interferometry* (ATI) is based on forming interferograms between the images, and detecting changes in the phase differences [39, chapter 7.3.2], [40] (similar to coherent change detection). Another approach is to subtract the images to suppress clutter (or unwanted signal), such that low signature changes can be more easily detected. This is known as *Displaced Phase Center Antenna* (DPCA) in SAR [41] (not to be confused with the DPCA technique reported in SAS [12] which is similar but used in another application). Both techniques have the potential to reduce the stationary signals such that a weak moving target signature can be detected. Exactly which approach is preferred, is dependent on the system, the geometry, and the application [42].

Most current SAS systems are multi-element receiver systems due to the along-track sampling criterion [2]. To obtain two or more fully populated synthetic apertures for along-track interferometry, the number of overlapping phase centers must be more than half the number of receiver channels. This is a major limitation, and such data were not recorded during the ARISE'12 trials.

F. Moving Target Synthetic Aperture Imaging

Moving targets in general do not obey the criterion for synthetic aperture imaging unless their velocity and trajectory is compensated for correctly [43]. The effect of assuming that the scene is stationary under the synthetic aperture image formation is that a moving target will be displaced and smeared. This is well-documented in SAR [39, chapter 7], [44, chapter

Dette er en postprint-versjon / This is a postprint version.
DOI til publisert versjon / DOI to published version: 10.1109/JOE.2014.2340351

5.2]. One potential way to estimate the motion of a feature in a synthetic aperture image is to apply time-frequency analysis on the feature in the image [39, chapter 7.3]. A moving target would induce a certain time-frequency relation that can be detected in certain cases. This is a technique that does not require multiple antennas, as the ATI/DPCA techniques do. Since the scene to be imaged (the seabed) is stationary, this technique will work poorly, and substantially worse than the ATI/DPCA techniques.

G. Doppler Estimation

The bolus phenomenon moves with a given speed. A potential technique is to estimate the speed directly from Doppler shift estimation (fast time) ideally on a single pulse-echo. The internal wave itself does not cause any backscattered signal but affects the acoustic signals in two ways: A refractive ray bending effect that moves the intensity distribution (not the scatterers); and a decrease in the wave speed through the moving feature which causes displacement of the scatterers in the image. This means that there is very little (fast time) Doppler shift of the signal which requires a relative velocity between transmitter-scatterer-receiver.

H. Defocusing Effect

A weaker but potentially detectable effect is the fact that the bolus transports water of lower sound speed. The acoustic signal propagating through the waves will cause defocusing in the SAS images if not compensated for. However, the traveled distance through the water with incorrect sound speed is short - on the order of a few meters, which again leads to very mild and maybe undetectable defocus. The primary effect of this will be the displacement described in Section III and not the defocus.

I. Summary of Techniques

In this section, we have listed some candidate techniques to detect and verify that a certain observable feature in a SAS image is caused by a water column effect. Based on a simple assessment of the techniques, our conclusions are the following:

- The techniques described in Sections IV-E, IV-F, IV-G, and IV-H will work poorly or not at all.
- The techniques described in Sections IV-B, IV-C, and IV-D have potential to work, but the detection will be difficult.
- The technique described in Section IV-A which includes data collections in repeated passes is preferred, and will provide sufficient data for accurate detection and potential characterization of the water column effects.

V. Conclusions

Synthetic aperture sonar (SAS) is a tool well suited for detailed investigations of the seabed. As with all other types of sonar, SAS may be affected by the ocean environment and the sound speed profile in particular. Internal waves are common in a layered ocean environment, possibly causing refractive effects for SAS. In this paper we have presented SAS images from repeated passes of the same area, where strong features apparently on the seabed were not present 28 hours later. To emphasize the effect of the phenomenon, we present a final data example in Fig. 16.

We have presented a simple geometrical theory that explains how a feature that results from a breaking internal wave (a bolus) can cause refractive effects that fit well with the observations. Hence, we believe the apparent strong features on the seabed are caused by a refracting water column effect. These features appear very similar to actual seabed topography in sidescan sonar images, SAS images, and SAS bathymetry. Such refractive effects from internal wave boluses can only occur when a strong density and sound speed step intersects a sloping seabed, and the sonar viewing geometry is advantageous.

We have presented different techniques to detect and distinguish these water column effects from real features on the seabed. The most favourable technique is to run repeated passes and perform noncoherent image-based change detection or differential interferometry. For cases when only single pass data are available, we have presented two techniques that potentially might prove successful: Multi-aperture processing and multi-look processing combined with displacement estimation. The phenomenon discussed in this paper moves very slowly, so that these techniques will require a relatively large temporal separation between looks.

For applications such as *change detection*, SAS is becoming a common tool. Operations in the littoral zone may be affected by ocean environmental variability. In such cases, it is important to distinguish between real features on the seabed and effects caused solely by the water column. In this paper, we have shown that the refractive effect of internal waves can cause strong features that resemble features on the seabed. Finally, the data presented in this paper strongly suggests that state-of-art SAS especially when collecting data in repeated passes, is sufficiently advanced to be used for detailed investigations of the oceanographic processes underlying the variations in water column properties.

Acknowledgements

The authors would like to thank NATO Centre for Maritime Research and Experimentation for hosting and organizing the ARISE'12 trial. The authors also thank the HUGIN AUV operators and researchers at Norwegian Defence Research Establishment for gathering the data. The authors are grateful to Stig Asle Vaksvik Synnes for his valuable insight on ray acoustics. The work performed by ARL-PSU was supported under ONR Grant No. N00014-13-1-0020. The work performed by GTRI was supported under ONR grant No. N00014-12-1-0085.

References

[1] M. P. Hayes and P. T. Gough, "Synthetic Aperture Sonar: A Review of Current Status," *IEEE J. Oceanic Eng.*, vol. 34, no. 3, pp. 207–224, July 2009.

[2] R. E. Hansen, "Introduction to Synthetic Aperture Sonar," in *Sonar Systems*, N. Z. Kolev, Ed. Intech, September 2011, ch. 1, pp. 3–28. [Online]. Available: http://www.intechopen.com/books/sonar-systems

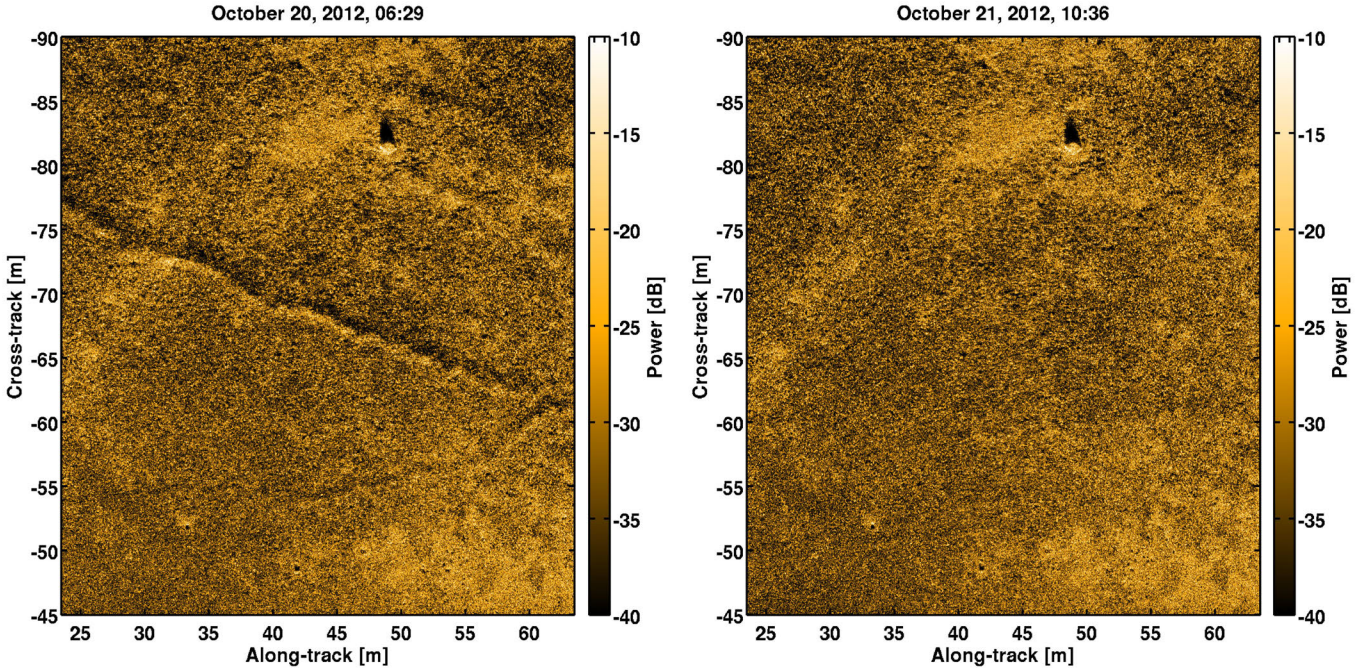

Fig. 16. SAS image taken of the same scene 28 hours apart. The left image is the earliest. The apparent small ridge in the earliest SAS image is water column induced, and completely vanished in the last SAS image. The other objects and the seabed texture are preserved and do not change significantly between the two passes.

[3] G. Franceschetti and R. Lanari, *Synthetic Aperture Radar Processing*. Boca Raton, FL, USA: CRC Press, 1999.

[4] D. Massonnet and J. Souyris, *Imaging with synthetic aperture radar*, ser. Engineering sciences. Lausanne, Switzerland: EFPL Press, 2008.

[5] D. D. Sternlicht, T. G-Michael, and C. A. Matthews, "Advances in seabed change detection for port and coastal security," in *Proceedings of the International Conference on Waterside Security*, May 2012.

[6] X. Lurton, *An Introduction to Underwater Acoustics: Principles and Applications*, 2nd ed. Chichester, UK: Springer Praxis Publishing, 2010.

[7] H. J. Callow, T. O. Sæbø, S. A. Synnes, and R. E. Hansen, "SAS beamforming through a vertical sound speed profile," in *Proceedings of Underwater Acoustic Measurements 2011*, Kos, Greece, June 2011.

[8] R. E. Hansen, H. J. Callow, T. O. Sæbø, and S. A. V. Synnes, "Challenges in Seafloor Imaging and Mapping with Synthetic Aperture Sonar," *IEEE Trans. Geosci. Remote Sens.*, vol. 49, no. 10, pp. 3677–3687, October 2011.

[9] F. S. Henyey, D. Rouseff, J. M. Grochocinski, S. A. Reynolds, K. L. Williams, and T. Ewart, "Effects of Internal Waves and Turbulence on a Horizontal Aperture Sonar," *IEEE J. Oceanic Eng.*, vol. 22, no. 2, pp. 270–280, April 1997.

[10] J. T. Christoff, C. D. Loggins, and E. L. Pipkin, "Measurement of the temporal phase stability of the medium," *J. Acoust. Soc. Am.*, vol. 71, no. 6, pp. 1606–1607, June 1982.

[11] P. T. Gough and M. P. Hayes, "Measurements of acoustic phase stability in Loch Linnhe, Scotland," *J. Acoust. Soc. Am.*, vol. 86, no. 2, pp. 837–839, August 1989.

[12] A. Bellettini and M. A. Pinto, "Theoretical accuracy of synthetic aperture sonar micronavigation using a displaced phase-center antenna," *IEEE J. Oceanic Eng.*, vol. 27, no. 4, pp. 780–789, October 2002.

[13] M. A. Pinto, "High Resolution Seafloor Imaging with Synthetic Aperture Sonar," *IEEE Oceanic Eng. Newsletter*, pp. 15–20, Summer 2002.

[14] K. R. Helfrich, " Internal solitary wave breaking and run-up on a uniform slope," *J. Fluid Mech.*, vol. 243, pp. 133–154, October 1992.

[15] B. C. Wallace and D. L. Wilkinson, "Run-up of internal waves on a gentle slope in a two-layered system," *J. Fluid Mech.*, vol. 191, pp. 419–442, June 1988.

[16] S. K. Venayagamoorthy and O. B. Fringer, "On the formation and propagation of nonlinear internal bolusess across a shelf break," *J. Fluid Mech.*, vol. 577, pp. 137–159, April 2007.

[17] D. Bourgault, M. D. Blokhina, R. Mirshak, and D. E. Kelley, "Evolution of a shoaling internal solitary wave train," *Geophys. Res. Lett.*, vol. 34, no. 3, February 2007.

[18] F. M. Dickey, J. M. DeLaurentis, and A. W. Doerry, "A SAR imaging model for large-scale atmospheric inhomogeneities," in *Proceedings of SPIE*, vol. 5410, August 2004, pp. 1–9.

[19] A. Muschinski, F. M. Dickey, and A. W. Doerry, "Possible effects of clear-air refractive-index perturbations on SAR images," in *Proc. SPIE*, vol. 5788, Orlando, FL, March 2005, pp. 25–33.

[20] F. M. Dickey, A. W. Doerry, and L. A. Romero, "Degrading effects of the lower atmosphere on long range SAR imaging," *IET Radar, Sonar Navig.*, vol. 1, no. 5, October 2007.

[21] P. E. Hagen, T. G. Fossum, and R. E. Hansen, "HISAS 1030: The Next Generation Mine Hunting Sonar for AUVs," in *UDT Pacific 2008 Conference Proceedings*, Sydney, Australia, November 2008.

[22] M. Preiss and N. J. S. Stacy, "Coherent Change Detection: Theoretical Description and Experimental Results," Defence Science and Technology (DSTO), Australia, Technical Report DSTO–TR–1851, Aug. 2006.

[23] J. C. V. Jakowatz, D. E. Wahl, P. H. Eichel, D. C. Ghiglia, and P. A. Thompson, *Spotlight-Mode Synthetic Aperture Radar: A Signal Processing Approach*. Dordrecht, The Netherlands: Kluwer Academic Publishers, 1996.

[24] T. O. Sæbø, S. A. V. Synnes, and R. E. Hansen, "Wideband Interferometry in Synthetic Aperture Sonar," *IEEE Trans. Geosci. Remote Sensing*, vol. 51, no. 8, pp. 4450–4459, August 2013.

[25] R. F. Hanssen, *Radar Interferometry: Data Interpretation and Error Analysis*. Dordrecht, The Netherlands: Kluwer Academic Publishers, 2001.

[26] L. Brekhovskikh and Y. Lysanov, *Fundamentals of Ocean Acoustics*, ser. Springer Series in Electrophysics. Berlin, Germany: Springer-Verlag, 1982, vol. 8.

[27] A. P. Lyons, R. E. Hansen, T. O. Sæbø, and H. J. Callow, "Refractive Effects of Internal Waves on Synthetic Aperture Sonar Images," in *Proceedings of the 1st Underwater Acoustic Conference*, Corfu, Greece, June 2013.

[28] D. Jackson and M. Richardson, *High-Frequency Seafloor Acoustics*. Springer-Verlag, 2007.

[29] "High-frequency ocean environment acoustic models handbook," Applied Physics Laboratory, University of Washington, Technical Report APL-UW TR 9407, 1994.

[30] T. O. Sæbø, "Seafloor Depth Estimation by means of Interferometric

Synthetic Aperture Sonar," Ph.D. dissertation, University of Tromsø, Norway, September 2010.
[31] Ø. Midtgaard, R. E. Hansen, T. O. Sæbø, V. Myers, J. R. Dubberley, and I. Quidu, "Change Detection Using Synthetic Aperture Sonar: Preliminary Results from the Larvik Trial," in *Proceedings of Oceans 2011 MTS/IEEE*, Kona, HI, USA, September 2011.
[32] A. P. Lyons and D. C. Brown, "The Impact of the Temporal Variability of Seafloor Roughness on Synthetic Aperture Sonar Repeat–Pass Interferometry," *IEEE J. Oceanic Eng.*, vol. 38, no. 1, pp. 91–97, January 2013.
[33] T. O. Sæbø, R. E. Hansen, H. J. Callow, and S. A. Synnes, "Coregistration of synthetic aperture sonar images from repeated passes," in *Proceedings of Underwater Acoustic Measurements 2011*, Kos, Greece, June 2011.
[34] J. E. Fernandez and J. T. Christoff, "Multi-Aspect Synthetic Aperture Sonar," in *Proceedings of Oceans 2000 MTS/IEEE*, Providence, RI, USA, September 2000, pp. 177–180.
[35] D. A. Cook, J. T. Christoff, and J. E. Fernandez, "Broadbeam Multi-Aspect Synthetic Aperture Sonar," in *Proceedings of Oceans 2001 MTS/IEEE*, Honolulu, HI, USA, November 2001, pp. 188–192.
[36] R. E. Hansen, H. J. Callow, T. O. Sæbø, P. E. Hagen, and B. Langli, "High fidelity synthetic aperture sonar products for target analysis," in *Proceedings of Oceans '08 Quebec*, Quebec, Canada, September 2008.
[37] K. Ouchi, "On the Multilook Images of Moving Targets by Synthetic Aperture Radars," *IEEE Trans. Antennas Propagat.*, vol. AP-33, no. 8, pp. 823–827, August 1985.
[38] E. Coiras, Y. Petillot, and D. M. Lane, "Multiresolution 3-D Reconstruction From Side-Scan Sonar Images," *IEEE Trans. Image Process.*, vol. 16, no. 2, pp. 382–390, February 2007.
[39] V. C. Chen and H. Ling, *Time-Frequency Transforms for Radar Imaging and Signal Analysis*. Boston, MA: Artech House, 2002.
[40] P. A. Rosen, S. Hensley, I. R. Joughin, F. K. Li, S. N. Madsen, E. Rodriguez, and R. M. Goldstein, "Synthetic Aperture Radar Interferometry," *Proc. IEEE*, vol. 88, no. 3, pp. 333–382, 2000.
[41] C. E. Muehe and M. Labitt, "Displaced-Phase-Center Antenna Technique," *Lincoln Laboratory Journal*, vol. 12, no. 2, pp. 281–296, 2000.
[42] S. Chiu and C. Livingstone, "A comparison of displaced phase centre antenna and along-track interferometry techniques for RADARSAT-2 ground moving target indication," *Can. J. Remote Sensing*, vol. 31, no. 1, pp. 37–51, February 2005.
[43] R. K. Raney, "Synthetic aperture radar (SAR) images of moving targets," *IEEE Trans. Aerosp. Electron. Syst.*, vol. AES-7, no. 3, pp. 499–505, May 1971.
[44] M. Soumekh, *Fourier Array Imaging*. Englewood Cliffs, NJ, USA: Prentice Hall, 1994.

Roy Edgar Hansen (M'07) received the M.Sc. degree in physics in 1992, and the Ph.D. degree in physics in 1999, both from the University of Tromsø, Norway. From 1992 to 2000 he was with the Norwegian research company TRIAD, working on multistatic sonar, multistatic radar, SAR and underwater communications. Since 2000, he has been working at the Norwegian Defence Research Establishment (FFI), Kjeller, Norway. He is currently principal scientist and team-leader for the autonomous underwater vehicle development and the synthetic aperture sonar development at FFI. He is also adjunct associated professor at Centre for Imaging at University of Oslo, Norway.

Anthony Lyons (M'96) received the B.S. degree (summa cum laude) in physics from the Henderson State University, Arkadelphia, AR, in 1988 and the M.S. and Ph.D. degrees in oceanography from Texas A&M University, College Station, in 1991 and 1995, respectively. He was a Scientist at the SACLANT Undersea Research Centre, La Spezia, Italy, from 1995 to 2000, where he was involved in a variety of projects in the area of environmental acoustics. Currently, he is a Senior Scientist at the Applied Research Laboratory, The Pennsylvania State University, State College, where he is engaged in studies of high-frequency acoustic interaction with the seafloor and sea surface. Dr. Lyons was awarded, with the recommendation of the Acoustical Society of America, the Institute of Acoustics (U.K.) A.B. Wood Medal for distinguished contributions in the underwater application of acoustics in 2003. He is a Fellow of the Acoustical Society of America and a member of the IEEE Oceanic Engineering Society.

Torstein Olsmo Sæbø (M'06-SM'13) was born in Bergen, Norway, in 1977. He received the cand.scient (M.Sc.) degree in astrophysics in 2002, from the University of Oslo, Norway. Since 2002, he has been working at the Norwegian Defence Research Establishment (FFI), Kjeller, Norway, specializing in the field of interferometry on synthetic aperture sonar. In 2010 he received the Ph.D degree in physics from the University of Tromsø, Norway, entitled Seafloor Depth Estimation by means of Interferometric Synthetic Aperture Sonar. He is currently senior scientist at FFI and also newly appointed associate editor for IEEE Journal of Oceanic Engineering.

Hayden John Callow (M'07) received the BE degree in 1998 from the University of Canterbury, Christchurch, New Zealand. Since completing his Ph.D. degree on synthetic aperture sonar (SAS) image enhancement with the Acoustics Research Group, University of Canterbury in 2003, he joined the Norwegian Defence Research Establishment in 2004 where he worked within the AUV research team on SAS imaging sensors, primarily performing research into SAS beamforming, micronavigation and interferometry. In 2011 he joined Kongsberg Maritime, where he works as a SAS R&D Engineer.

Daniel A. Cook (M'07-SM'08) received the B.S. and M.S. degrees in mechanical engineering and the M.S. degree in electrical and computer engineering from the Georgia Institute of Technology, Atlanta, in 1998, 2000, and 2007, respectively. From 2000 to 2007, he was with the Naval Surface Warfare Center, Panama City, FL, where he developed techniques for synthetic aperture sonar motion estimation and compensation. Currently, he is with the Sensors and Electromagnetic Applications Laboratory, Georgia Tech Research Institute (GTRI/SEAL), where his research is in the area of SAR imaging and adaptive radar signal processing.

Dette er en postprint-versjon / This is a postprint version.
DOI til publisert versjon / DOI to published version: 10.1109/JOE.2014.2340351